Fabrication and characterization of porous-core honeycomb bandgap THz fibers

Bao, Hualong; Nielsen, Kristian; Rasmussen, Henrik K.; Jepsen, Peter Uhd; Bang, Ole

Published in:
Optics Express

Link to article, DOI:
10.1364/OE.20.029507

Publication date:
2012

Document Version
Publisher's PDF, also known as Version of record

Fabrication and characterization of porous-core honeycomb bandgap THz fibers

Hualong Bao,[1] Kristian Nielsen,[1] Henrik K. Rasmussen,[2] Peter Uhd Jepsen,[1,*] and Ole Bang[1,3]

[1]*DTU Fotonik - Department of Photonics Engineering, Technical University of Denmark, Dk-2800 Kongens Lyngby, Denmark*

[2]*DTU Mekanik - Department of Mechanical Engineering, Technical University of Denmark, Dk-2800 Kongens Lyngby, Denmark*

[3]*oban@fotonik.dtu.dk*

**puje@fotonik.dtu.dk*

Abstract: We present a numerical and experimental investigation of a low-loss porous-core honeycomb fiber for terahertz wave guiding. The introduction of a porous core with hole size of the same dimension as the holes in the surrounding honeycomb cladding results in a fiber that can be drawn with much higher precision and reproducibility than a corresponding air-core fiber. The high-precision hole structure provides very clear bandgap guidance and the location of the two measured bandgaps agree well with simulations based on finite-element modeling. Fiber loss measurements reveal the frequency-dependent coupling loss and propagation loss, and we find that the fiber propagation loss is much lower than the bulk material loss within the first band gap between 0.75 and 1.05 THz.

OCIS codes: (060.5295) Photonic crystal fibers; (230.7370) Waveguides.

References and links

1. J. A. Harrington, R. George, P. Pedersen, and E. Mueller, "Hollow polycarbonate waveguides with inner Cu coatings for delivery of terahertz radiation," Opt. Express **12**(21), 5263–5268 (2004).
2. B. Bowden, J. A. Harrington, and O. Mitrofanov, "Fabrication of terahertz hollow-glass metallic waveguides with inner dielectric coatings," J. Appl. Phys. **104**(9), 093110 (2008).
3. B. Bowden, J. A. Harrington, and O. Mitrofanov, "Silver/polystyrene-coated hollow glass waveguides for the transmission of terahertz radiation," Opt. Lett. **32**(20), 2945–2947 (2007).
4. K. L. Wang and D. M. Mittleman, "Metal wires for terahertz wave guiding," Nature **432**(7015), 376–379 (2004).
5. K. Nielsen, H. K. Rasmussen, A. J. L. Adam, P. C. M. Planken, O. Bang, and P. U. Jepsen, "Bendable, low-loss Topas fibers for the terahertz frequency range," Opt. Express **17**(10), 8592–8601 (2009).
6. K. Nielsen, H. K. Rasmussen, P. U. Jepsen, and O. Bang, "Broadband terahertz fiber directional coupler," Opt. Lett. **35**(17), 2879–2881 (2010).
7. L. J. Chen, H. W. Chen, T. F. Kao, J. Y. Lu, and C. K. Sun, "Low-loss subwavelength plastic fiber for terahertz waveguiding," Opt. Lett. **31**(3), 308–310 (2006).
8. H.-W. Chen, Y.-T. Li, C.-L. Pan, J.-L. Kuo, J.-Y. Lu, L.-J. Chen, and C.-K. Sun, "Investigation on spectral loss characteristics of subwavelength terahertz fibers," Opt. Lett. **32**(9), 1017–1019 (2007).
9. H. Han, H. Park, M. Cho, and J. Kim, "Terahertz pulse propagation in a plastic photonic crystal fiber," Appl. Phys. Lett. **80**(15), 2634–2636 (2002).
10. A. Hassani, A. Dupuis, and M. Skorobogatiy, "Porous polymer fibers for low-loss Terahertz guiding," Opt. Express **16**(9), 6340–6351 (2008).
11. S. Atakaramians, A. V. Shahraam, B. M. Fischer, D. Abbott, and T. M. Monro, "Porous fibers: A novel approach to low loss THz waveguides," Opt. Express **16**(12), 8845–8854 (2008).
12. S. Atakaramians, S. Afshar, B. M. Fischer, D. Abbott, and T. M. Monro, "Low loss, low dispersion and highly birefringent terahertz porous fibers," Opt. Commun. **282**(1), 36–38 (2009).
13. S. Atakaramians, S. Afshar V, H. Ebendorff-Heidepriem, M. Nagel, B. M. Fischer, D. Abbott, and T. M. Monro, "THz porous fibers: design, fabrication and experimental characterization," Opt. Express **17**(16), 14053–14062 (2009).
14. S. Atakaramians, A. V. Shahraam, M. Nagel, H. K. Rasmussen, O. Bang, T. M. Monro, and D. Abbott, "Direct probing of evanescent fields for characterization of porous terahertz fibers," Appl. Phys. Lett. **98**(12), 121104 (2011).
15. C.-H. Lai, Y.-C. Hsueh, H.-W. Chen, Y.-J. Huang, H.-C. Chang, and C.-K. Sun, "Low-index terahertz pipe waveguides," Opt. Lett. **34**(21), 3457–3459 (2009).

#177934 - $15.00 USD Received 11 Oct 2012; revised 30 Nov 2012; accepted 3 Dec 2012; published 19 Dec 2012

16. C.-H. Lai, B. You, J.-Y. Lu, T.-A. Liu, J.-L. Peng, C.-K. Sun, and H.-C. Chang, "Modal characteristics of antiresonant reflecting pipe waveguides for terahertz waveguiding," Opt. Express **18**(1), 309–322 (2010).
17. J.-T. Lu, Y.-C. Hsueh, Y.-R. Huang, Y.-J. Hwang, and C.-K. Sun, "Bending loss of terahertz pipe waveguides," Opt. Express **18**(25), 26332–26338 (2010).
18. E. Nguema, D. Férachou, G. Humbert, J.-L. Auguste, and J.-M. Blondy, "Broadband terahertz transmission within the air channel of thin-wall pipe," Opt. Lett. **36**(10), 1782–1784 (2011).
19. J.-Y. Lu, C.-P. Yu, H.-C. Chang, H.-W. Chen, Y.-T. Li, C.-L. Pan, and C.-K. Sun, "Terahertz air-core microstructure fiber," Appl. Phys. Lett. **92**, 064105 1–3 (2008).
20. C. S. Ponseca, Jr., R. Pobre, E. Estacio, N. Sarukura, A. Argyros, M. C. J. Large, and M. A. van Eijkelenborg, "Transmission of terahertz radiation using a microstructured polymer optical fiber," Opt. Lett. **33**(9), 902–904 (2008).
21. A. Dupuis, K. Stoeffler, B. Ung, C. Dubois, and M. Skorobogiaty, "Transmission measurements of hollow-core THz Bragg fibers," J. Opt. Soc. Am. B **28**(4), 896–907 (2011).
22. B. Ung, A. Dupuis, K. Stoeffler, C. Dubois, and M. Skorobogatiy, "High-refractive-index composite materials for terahertz waveguides: trade-off between index contrast and absorption loss," J. Opt. Soc. Am. B **28**(4), 917–921 (2011).
23. Z. Wu, W.-R. Ng, M. E. Gehm, and H. Xin, "Terahertz electromagnetic crystal waveguide fabricated by polymer jetting rapid prototyping," Opt. Express **19**(5), 3962–3972 (2011).
24. K. Nielsen, H. K. Rasmussen, P. U. Jepsen, and O. Bang, "Porous-core honeycomb bandgap THz fiber," Opt. Lett. **36**(5), 666–668 (2011).
25. B. Ung, A. Mazhorova, A. Dupuis, M. Rozé, and M. Skorobogatiy, "Polymer microstructured optical fibers for terahertz wave guiding," Opt. Express **19**(26), B848–B861 (2011).
26. M. Rozé, B. Ung, A. Mazhorova, M. Walther, and M. Skorobogatiy, "Suspended core subwavelength fibers: towards practical designs for low-loss terahertz guidance," Opt. Express **19**(10), 9127–9138 (2011).
27. J. Anthony, R. Leonhardt, A. Argyros, and M. C. J. Large, "Characterization of a microstructured Zeonex terahertz fiber," J. Opt. Soc. Am. B **28**(5), 1013–1018 (2011).
28. A. Hassani, A. Dupuis, and M. Skorobogatiy, "Low loss porous terahertz fibers containing multiple subwavelength holes," Appl. Phys. Lett. **92**(7), 071101 (2008).
29. A. Dupuis, J.-F. Allard, D. Morris, K. Stoeffler, C. Dubois, and M. Skorobogatiy, "Fabrication and THz loss measurements of porous subwavelength fibers using a directional coupler method," Opt. Express **17**(10), 8012–8028 (2009).
30. M. Nagel, A. Marchewka, and H. Kurz, "Low-index discontinuity terahertz waveguides," Opt. Express **14**(21), 9944–9954 (2006).
31. J. Anthony, R. Leonhardt, S. G. Leon-Saval, and A. Argyros, "THz propagation in kagome hollw-core microstructured fibers," Opt. Express **19**(19), 18470–18478 (2011).
32. M. C. J. Large, L. Poladian, G. Barton, and M. A. van Eijkelenborg, *Microstructured polymer optical fibres*, (Springer, 2008).
33. J. Broeng, S. E. Barkou, A. Bjarklev, J. C. Knight, T. A. Birks, and P. St. J. Russell, "Highly increased photonic band gaps in silica/air structures," Opt. Commun. **156**(4-6), 240–244 (1998).
34. J. C. Knight, J. Broeng, T. A. Birks, and P. St. J. Russell, "Photonic band gap guidance in optical fibers," Science **282**(5393), 1476–1478 (1998).
35. W. Yuan, L. Khan, D. J. Webb, K. Kalli, H. K. Rasmussen, A. Stefani, and O. Bang, "Humidity insensitive TOPAS polymer fiber Bragg grating sensor," Opt. Express **19**(20), 19731–19739 (2011).
36. G. Emiliyanov, J. B. Jensen, O. Bang, P. E. Hoiby, L. H. Pedersen, E. M. Kjaer, and L. Lindvold, "Localized biosensing with Topas microstructured polymer optical fiber," Opt. Lett. **32**(5), 460–462 (2007).
37. P. U. Jepsen, D. G. Cooke, and M. Koch, "Terahertz spectroscopy and imaging – Modern techniques and applications," Laser & Photon. Rev. **5**(1), 124–166 (2011).

1. Introduction

Waveguides and functional devices for terahertz (THz) operational frequencies have been extensively investigated recently, both based on metals [1–4] and dielectrics [5–31]. However, THz waveguides still demonstrate orders of magnitude higher loss than their near-infrared counterparts, and thus common to most waveguide studies is the quest for lower propagation loss, typically limited by finite metallic conductivity or dielectric losses.

It is well known that dry air is the most transparent medium in the THz regime. In order to lower the propagation loss of a THz waveguide, an effective approach is therefore to maximize the fraction of the power propagating in air, while at the same time maintaining a tight confinement of the propagating mode. Several methods towards this have been proposed. One strategy first demonstrated by Chen *et al.* is to use a subwavelength core surrounded by an air cladding [7,8]. In order to further reduce the loss, a porous structure of sub-wavelength holes can be introduced into the already sub-wavelength solid core of the fiber [10–14,28–30], as first predicted numerically by Hassani *et al.* [10,28] and then demonstrated by Dupuis *et al.* [29] and later Atakaramians *et al.* [13]. Due to the boundary

#177934 - $15.00 USD Received 11 Oct 2012; revised 30 Nov 2012; accepted 3 Dec 2012; published 19 Dec 2012

conditions in the electric flux density the refractive index step between material and air in the sub-wavelength holes pushes the field into the lower index holes, thereby increasing the fraction of power in air and reducing the absorption losses [30]. Propagation losses as low as 0.04 dB/cm near 0.3THz have been reported [29].

However, irrespective of the fine details of the design, such sub-wavelength air-clad fibers are still limited in their practical applicability due to their susceptibility to perturbations. One way to shield the fiber from external perturbations is to have it be the core of a so-called suspended core fiber, as reported by Rozé *et al.* [26], who demonstrated losses less than 0.09 dB/cm in the 0.28-0.48 THz range. This design has the added advantage that the three large holes constituting the air cladding may be purged with dry air to avoid losses due to moisture. The suspended core type THz fiber can be made to have a porous core, but this has only been demonstrated for relatively large cores [26]. One disadvantage of the suspended-core THz fiber is that it is rather difficult to cleave.

Another strategy is to use hollow-core waveguides. In this type of waveguides most of the THz field is guided within the air-core region, and consequently propagation loss and environmental disturbance can be significantly reduced. Different designs have been realized, such as pipe waveguides [15–18] and photonic bandgap (PBG) fibers with a hexagonal cladding hole structure [19,23] or an omnidirectional Bragg-stack type cladding with rings of hole structures [20] or continuous layers of alternating materials [20–22]. PBG fibers are particularly versatile candidates for THz waveguiding due to the flexibility in the design of critical parameters such as center frequency, bandwidth, and dispersion. Here we focus on the PBG THz fiber.

The fabrication of the first PBG THz fiber was reported in 2008 by Lu *et al.* [19], who stacked 20 cm long Teflon tubes with inner/outer diameters from 0.81/1.11 mm to 1.68/2.08 mm in a close hexagonal structure with lattice constant Λ = 2.08 mm and used thin heat-shrinkable polyethylene tubes to keep the Teflon tubes together. After stacking the central 7 Teflon tubes were removed to form the hollow core. This preform was used directly as a THz fiber without drawing or fusing to reduce the diameter and thus the fiber outer diameters were very large (~20 mm). A minimum loss of 0.01 dB/cm was reported, but this was in an extremely narrow frequency band less than 20 GHz wide around 770 GHz. In fact no real bandgaps were observed and the authors instead attributed the guiding mechanism to antiresonant reflecting optical waveguiding (ARROW). Not surprisingly the demonstrated hole structures were close to perfect, but evidently this type of large diameter PBG fiber is not practical and cannot be cleaved or bent.

Later in 2008 Ponseca *et al.* [20] reported the first Bragg-type PBG THz fiber fabricated by drilling one large center hole and 5 rings of small holes around it into a 7 cm in diameter PMMA polymer rod and drawing it down to a THz fiber with approximately 6 mm diameter. The fiber with the lowest loss of 0.9 dB/cm at 1.3 THz had a core diameter of 670 μm and hole diameters of 65μm. The distance or pitch between holes in the same ring and in neighbouring rings was Λ_i = 86 μm and Λ_e = 93 μm, respectively. Importantly, the difficulties in maintaining the preform structure when drawing structures with such different sizes of airholes were very apparent. Thus draw-induced deformations resulted in elliptical holes and a chirp in both hole diameters and Λ_e with values that varied by 15% from the innermost to the outermost ring. Such deformations are well-known also from the more developed technology of microstructured Polymer Optical Fibers (mPOFs) for transmission in the visible [32].

In 2011 Wu *et al.* used polymer jetting rapid prototyping to make 5-15 cm long PBG THz fibers with a large hollow core and hexagonal cladding hole structure [23]. A minimum loss of 0.3 dB/cm at 105 GHz was reported in a fiber with outer diameter 40 mm, core diameter 8.4 mm, pitch 3 mm, and hole diameter 2.6 mm. This special fabrication technique gave perfect hole structures, but imposes a minimum feature size of 0.1-0.15 mm. Due to the huge structure the transmission displayed no real bandgaps, but narrow resonances below 240 GHz. As with the simple stacking the large structures achieved with the polymer jetting technique does not provide practical THz fibers working above 1 THz that may be easily bent, cleaved, and mass fabricated in long lengths.

#177934 - $15.00 USD Received 11 Oct 2012; revised 30 Nov 2012; accepted 3 Dec 2012; published 19 Dec 2012

In the same year, Anthony *et al.* reported the fabrication of a PMMA kagome hollow-core fiber using standard fiber drawing [31]. A loss of around 2.6 dB/cm over 0.65-1.0 THz with a minimum loss of approximately 1 dB/cm around 1 THz was reported in a fiber with outer diameter of 6.8 mm and core diameter of 2.2 mm. The vastly different hole sizes in the preform makes the kagome fiber difficult to draw and consequently the drawn fiber structure was strongly perturbed.

Finally, in 2011, Dupuis *et al.* [21] and Ung *et al.* [22] reported on the fabrication of Bragg-type PBG fibers consisting of alternating layers of polymer and air and of polymer and polymer composite. The preform was rolled from thin sheets of polymer and solidified in an oven to give 22.5 cm long fibers with an inner hollow core diameter of 6.6 mm. Several broad transmission bands with loss below 1 dB/cm were observed in the 0.1-2.0 THz regime with the minimum loss being less than 0.12 dB/cm (0.18 dB/cm) for the polymer/air (polymer/polymer) Bragg fiber in the region 0.7-0.8 THz. However, the fibers were so fragile that they could not be cleaved or bent.

Looking at the state-of-the-art in fabricated THz PBG fibers [19–23], no fiber has yet been reported, which has good broadband transmission around 1 THz, may be bent and cleaved, and which can be (mass) fabricated in long length. The stacking + tubing [19] and polymer jetting [23] techniques provide good periodic (hexagonal) hollow-core PBG structures, but at the expense of very thick fibers that do not display broadband low loss guiding and do not easily allow bending, cleaving and fabrication of long lengths. The rolling + solidification technique [21,22] can make low loss PBG Bragg fibers, but the fibers are very big and extremely fragile. The only technique that allows mass fabrication of long lengths of THz fiber is conventional fiber drawing [20] (see also [10,27] for solid-core THz fibers). However, good-quality hollow-core PBG THz fibers have so far been difficult to draw due to the different expansion rates of holes of different diameter at elevated temperatures, which leads to deformation of the smaller holes during the drawing process, unless special precautions are taken. The imbalance of hole dimensions can to some extent be alleviated by applying pressure to the holes during drawing. However, such a procedure can only be applied to a limited extent and obviously adds to the complexity of fabrication

In 2011 we used numerical modeling to propose a PBG THz fiber type, which combined PBG guidance with the concept of porous waveguides, to provide preforms consisting of identical holes with the same diameter. Basically it consists of a hollow-core PBG THz fiber cladding structure with a porous core inserted into the hollow core [24]. This allows PBG guidance, while still keeping the loss low due to the porous core. Due to the increased effective index of the core, the cladding PBG structure is a honeycomb structure, which from optical fibers is known to more easily allow broad bandgaps [33,34].

Here we present the first fabrication and experimental characterization of such a PBG THz fiber made of the polymer TOPAS and confirm that it allows to fabricate long lengths of fiber with a near-perfect periodic structure and thus very clear bandgap guidance. The fundamental bandgap at 0.75-1.05 THz is found to have losses lower than 1.5 dB/cm, whereas the loss is below 1.0 dB/cm in the reduced bandgap 0.78-1.02 THz. The particular fiber we present has an outer diameter of 3.65 mm, and is thus already flexible. The outer diameter can be further reduced and thus these fibers may also be bent and cleaved. The polymer TOPAS used as fiber material, is chosen because of its many advantageous properties, which include low loss and dispersion at THz frequencies [5] and the fact that it is humidity insensitive [35] and chemically inert with special biosensing properties [36].

2. Fiber fabrication

Figure 1(a) shows the idealized structure of the proposed porous-core honeycomb bandgap terahertz fiber for simulation and Fig. 1(b) shows a microscope image of the end facet of the fabricated fiber. The fiber consists of a honeycomb lattice of air holes with hole diameter d, and lattice pitch Λ, D_c is the effective core diameter, and D is the outer diameter of the whole fiber.

#177934 - $15.00 USD Received 11 Oct 2012; revised 30 Nov 2012; accepted 3 Dec 2012; published 19 Dec 2012

The low-index porous core (indicated by green circle in Fig. 1(a)) is formed by introducing a hexagonal array of air holes with the same diameter as the holes in the cladding. We fabricated the proposed fiber by using a cyclic olefin copolymer (COC) with the trade name TOPAS® COC 8007, obtained from Topas Advanced Polymers, Inc. The polymer granulates were cased into cylinders and then used as preforms. The desired photonic crystal hole structure was drilled into the polymer preform, and this structure was then preserved throughout the drawing process.

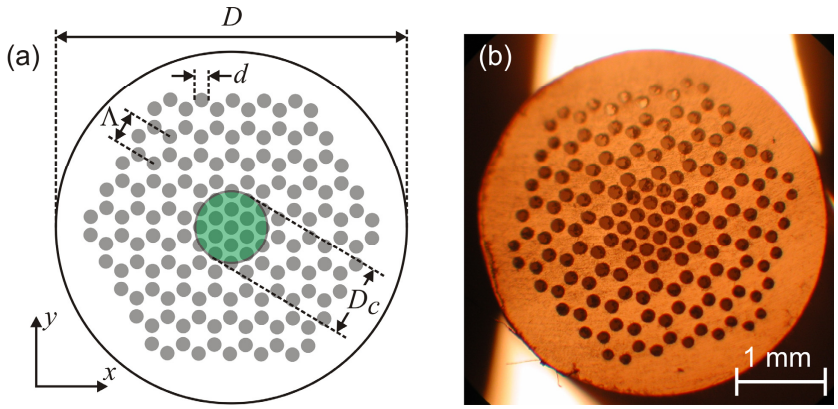

Fig. 1. (a) Idealized structure used in the simulation. (b) Microscope image of the actual fiber. Dark regions represent air and green central region in (a) represents the low index porous core region. d = 165 μm, Λ = 360 μm, D_c = 0.8 mm.

The bulk dielectric properties (absorption coefficient and refractive index) of TOPAS® were characterized by THz time-domain spectroscopy (THz-TDS) [37] on a disk with a thickness of 0.9992 cm and a diameter of 6 cm. The absorption coefficient and index of refraction are shown in Fig. 2.

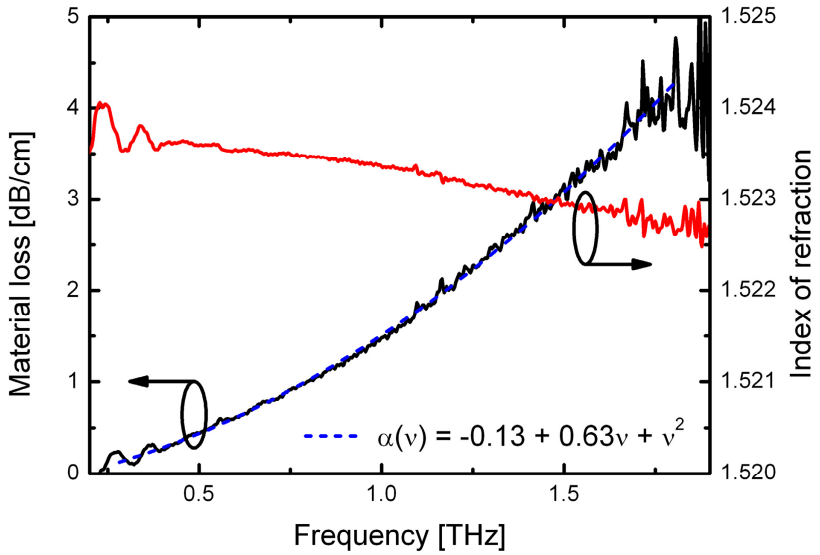

Fig. 2. Refractive index (red curve) and material loss (black curve) of the TOPAS® polymer used for fiber fabrication, measured on a disk with a thickness of 0.9992 cm and a diameter of 6.0 cm. Blue dashed curve is a phenomenological quadratic fit to the loss used in Fig. 8.

The material has an almost constant refractive index in the 0.2-2 THz range (near 1.5235, in excellent agreement with previously reported values [5]) and low loss (<1 dB/cm up to 0.8 THz, and <4 dB/cm up to 2 THz).

#177934 - $15.00 USD Received 11 Oct 2012; revised 30 Nov 2012; accepted 3 Dec 2012; published 19 Dec 2012

The honeycomb-cladding, limited to three rings by the diameter of the preform, and the porous core structure was drilled into the preform and then drawn to the final diameter. The structure is preserved during the drawing process and Fig. 1(b) shows a cross-sectional image of the fabricated THz fiber. The following parameters describe the fabricated THz fiber: D = 3.65 mm, d = 165 μm, Λ = 360 μm, and D_c = 0.8 mm. These are average values, with very small fluctuations across the fiber, as evident from Fig. 1(b).

3. Simulation and experimental results

Simulation of the fabricated fiber were carried out by using commercial software based on the plane-wave method (BandSolve, RSoft Design) for the band gap of the cladding unit cell and the commercially available FEM solver (COMSOL3.5a) for the fundamental core mode of the fiber. The resulting two band gaps are shown in gray in Fig. 3. The full geometry of the fiber was considered, including the finite outer diameter D. A 1 mm thick layer of air was placed around the fiber, again surrounded by a perfectly matched layer (PML) to be able to calculate the confinement loss. The resulting frequency-dependent effective refractive index of the fundamental mode in the two band gaps is shown in Fig. 3 (black curve), and the frequency-dependent fraction of the total power of the fundamental mode that is localized within the core region is shown in Fig. 4 (red curve). The small insets in Fig. 3 show the S_z energy flux distribution of the fundamental mode of the fiber at four different frequencies (0.7, 0.9, 1.4 and 1.6 THz). Numerous sharp resonant features are visible in the core power ratio, indicative (as will be discussed below) of resonant coupling between the reflected field from the outer interface of the fiber and the core mode. To illustrate this coupling, the two insets in Fig. 4 show the S_z energy flux distribution of the fundamental modes at two nearby frequencies at 0.80 THz (with low core power ratio) and at 0.82 THz (high core power ratio). Comparison of these two insets shows that at specific resonant frequencies, a large fraction of the power is located near the outer perimeter of the fiber, while the mode profile away from these resonances is confined to the core region.

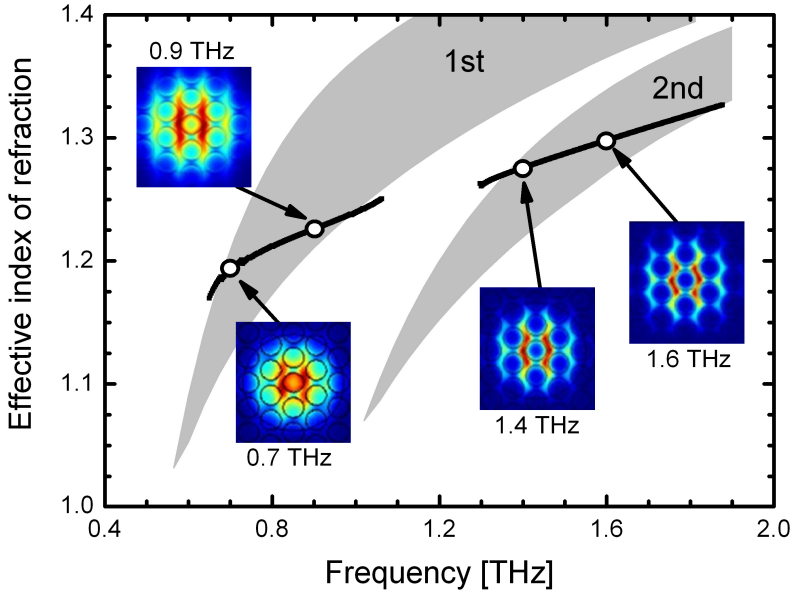

Fig. 3. Calculated bandgaps (grey zones) and effective index of the fundamental mode (black curves). Insets show the S_z energy flux distribution of the fundamental mode at four different frequencies (0.7, 0.9, 1.4 and 1.6 THz). The scale of each inset is 885 × 960 μm.

To shed further light on the effect of a finite fiber diameter and the effect of the reflection at the fiber/air interface we performed simulations where we eliminated the reflective polymer/air interface by applying a PML directly to the outer surface of the TOPAS fiber,

#177934 - $15.00 USD Received 11 Oct 2012; revised 30 Nov 2012; accepted 3 Dec 2012; published 19 Dec 2012

thereby effectively modeling an infinitely large fiber. The calculated frequency dependent core power ratio of the fundamental mode is shown in Fig. 4 (blue curve). The band gaps are identical to the finite fiber simulation discussed previously (red curve). However, the infinite fiber simulation lacks the resonant coupling between the core mode and the outer diameter of the fiber, resulting in a consistent high power fraction in the core region within the two band gaps.

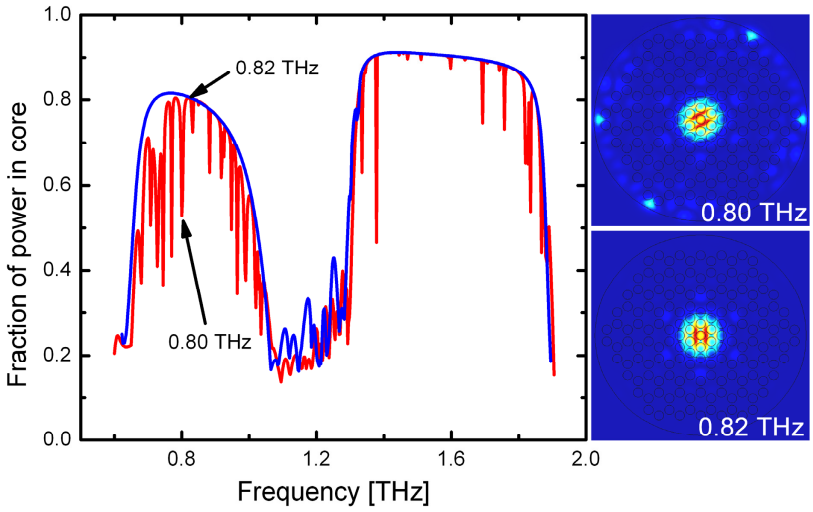

Fig. 4. Calculated fraction of power localized in the core of the honeycomb fiber with TOPAS (blue curve) and air (red curve) surrounding the fiber surface. The two insets to the right show the S_z energy flux distribution of the fundamental modes at nearby frequencies. One is at a resonant frequency due to reflection from the fiber/air interface (0.80 THz) and the other shows a well-confined mode (0.82 THz). The dimensions of the insets are 3.65 × 3.65 mm.

For experimental characterization of the fabricated fibers we performed transmission measurements with a commercial fiber-coupled THz-TDS system (Picometrix T-Ray 4000) with an effective spectral range 0.1-2.0 THz, determined by losses in the 1-in. focal length polymer lenses used for focusing of the THz pulses into the TOPAS fibers. The entrance facet of the fiber was placed immediately behind a small, variable aperture (~0.8-0.9 mm diameter) in the focal plane of the tightly focused THz beam. The aperture ensured a preferential excitation of core modes in the fiber. The THz signal transmitted through the fiber was detected by the THz receiver head of the Picometrix system, aligned with the fiber exit facet in its focal plane.

The reference pulse transmitted through the aperture is shown in Fig. 5(a), and consists mainly of a single cycle of the electric field. The time trace of THz pulses after propagation through a 5-cm long segment of fiber is shown in Fig. 5(b) (blue curve). The THz waveform transmitted through the fiber is dispersed in the time domain. As discussed above, we see numerical indication of strong interaction between cladding modes and core modes for finite-diameter fibers. In order to get more detailed information on this coupling we repeated the transmission experiment while adding some water (a strong absorber at THz frequencies) around the fiber surface. The transmitted pulse in this situation is shown as the red curve in Fig. 5(b). We observe significantly less pronounced oscillations at times later than 20 ps, while the initial part of the transmitted pulse is much less influenced by the absorbing water layer around the fiber. Further insight is obtained by performing a short-time Fourier transform (STFT) of the two time-domain traces in Fig. 5(b), as shown in Fig. 5(c) and 5(d), representing the transmission through the fiber surrounded by air and water, respectively. The frequencies below approximately 0.6 THz are attenuated by adding a layer of water, while the transmission in the two band gaps in the 0.7-1.1 THz and 1.3-1.7 THz regions are unaffected

#177934 - $15.00 USD Received 11 Oct 2012; revised 30 Nov 2012; accepted 3 Dec 2012; published 19 Dec 2012

by the water, clearly demonstrating that the absorptive water layer effectively strips the cladding modes from the fiber.

Based on the effective index shown in Fig. 3 we can calculate the arrival time of the various frequency components within the two band gaps after propagation through the 50-mm fiber section. The group delay is given by $t_g = n_g L / c$, where the group index is calculated from the effective propagation index as $n_g = n_{eff} + \nu \cdot dn_{eff} / d\nu$. This group delay is shown in Fig. 5(c) and 5(d) as black squares (identical data sets). There is excellent agreement between the simulated and the observed arrival time of the frequency components, and in particular the experiment reproduces the steep dispersion at the lowest frequencies of the first band gap as well as the delayed arrival of the signal in the second band gap.

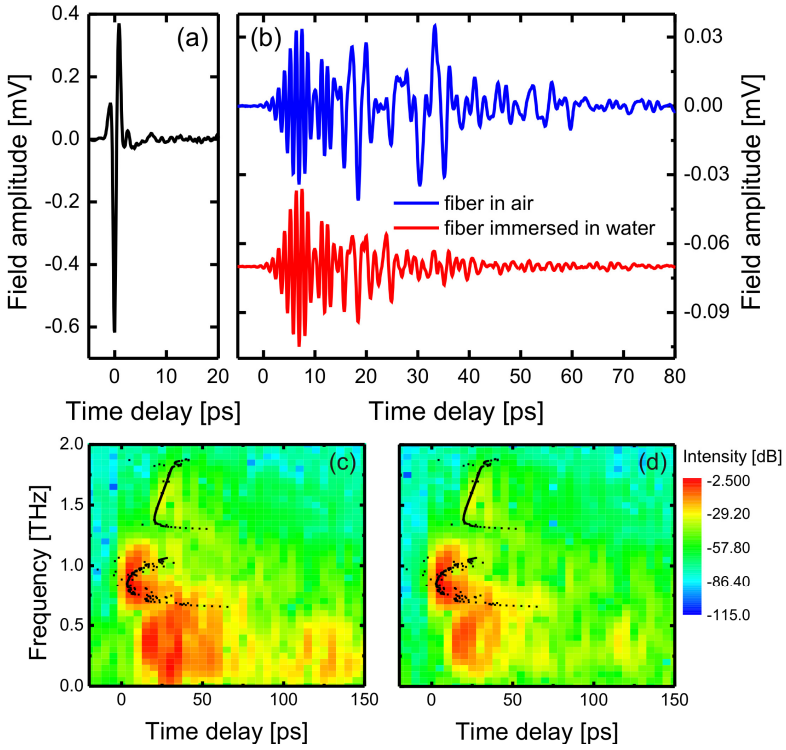

Fig. 5. Measured THz pulse for (a) reference signal (black curve) and (b) transmitted pulse through a 5 cm long honeycomb fiber with water (red curve) and air (blue curve) around the surface. Short-time Fourier transforms of the transmitted waveforms in (b) are shown in (c) and (d), respectively, with simulated group velocity arrival times of the spectral components overlaid.

Figure 6 quantifies the experimental transmission spectrum after transmission through the 5 cm long fiber segment, calculated as the ratio of the Fourier transforms of the signals in Fig. 5(b) and 5(a). After adding water around the fiber surface to attenuate cladding modes, transmission in the regions outside the band gaps (below 0.6 THz and between 1.1 and 1.3 THz) is reduced (red curve compared to black curve), as already indicated in the STFT trace in Fig. 5(d). The location of the two transmission band are in good agreement with the simulation (blue curve), which shows the fraction of the power residing on the core region, and thus indicates confinement of the field by the bandgap effect. The small discrepancy between predicted and observed bandgap positions may be caused by the small non-uniformity along the fiber length and imperfect uniformity of air-hole diameters across the fiber.

#177934 - $15.00 USD Received 11 Oct 2012; revised 30 Nov 2012; accepted 3 Dec 2012; published 19 Dec 2012

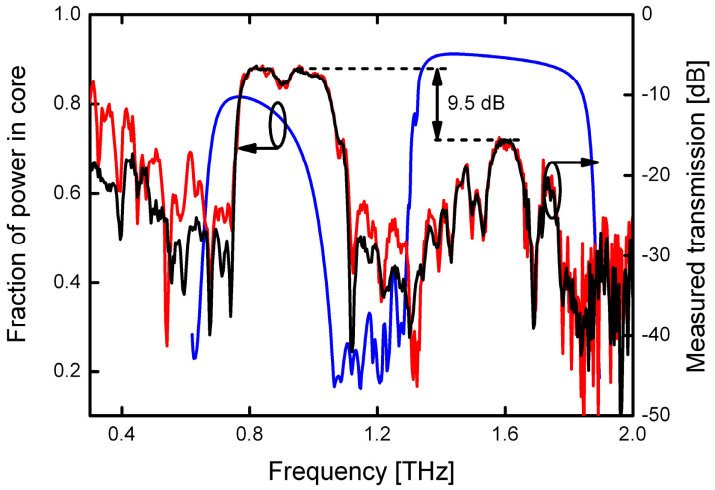

Fig. 6. Calculated fraction of power localized in the core of the honeycomb fiber with the TOPAS PML (blue curve). Measured relative transmission of the honeycomb fiber with air (red curve) and with water (black curve) around the fiber surface.

Importantly the experimental transmission spectra in Fig. 6 (red and black curves) show that transmission in the second band gap is much lower (approximately 9.5 dB) than that of the first band gap. To investigate this strong attenuation we calculated the fraction of power in the polymer material (green circles in Fig. 7) and multiplied this fraction with the measured material absorption coefficient (Fig. 2) to obtain the effective material loss due to absorption of light in the polymer (red circles in Fig. 7). As indicated in Fig. 7 we see that the fiber displays much higher material absorption loss (approximately 1.5 dB/cm, corresponding to 7.5 dB for the 5 cm fiber length) in the second band gap compared to the first band gap. The fact that the fraction of power in the polymer and thus the effective material loss is seen to increase with frequency is because of the porous core of our honeycomb bandgap fiber, which confines more and more of the light into the solid material between the holes as the wavelength gets smaller [10,11]. Additional attenuation may be caused by the smaller overlap integral between the free-space mode and the mode profile in the second band (see Fig. 3) compared to the first band gap.

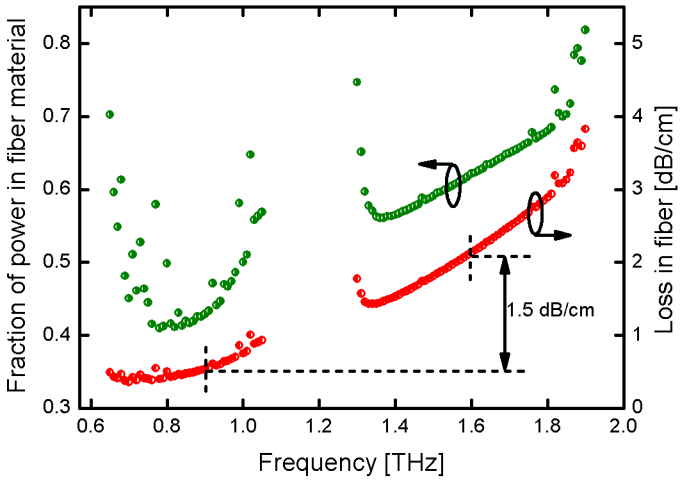

Fig. 7. Calculated fraction of power in the fiber material (green half-solid circle) and material loss in fiber (red half-solid circle), respectively.

#177934 - $15.00 USD Received 11 Oct 2012; revised 30 Nov 2012; accepted 3 Dec 2012; published 19 Dec 2012

The dips in the transmission spectrum in the second band gap may be caused by interference between the fundamental mode and higher order modes. Such interference is not observed in the first band gap. This may be due to the fact that coupling to the fundamental mode in the second band gap is more sensitive to alignment than in the first band gap, and slight off-center coupling could lead to an increased fraction of power being coupled into higher order modes.

Finally we discuss fiber loss measurements. The measurements were performed with a cutback method where transmission was measured on the same piece of fiber (initially 15 cm long), sequentially cut shorter in steps of 2.5 cm and repositioned in the experimental setup. Gentle milling after cleaving assured a uniform and high quality of the cleaved facet at each measurement. Care was taken to assure the same rotational orientation of the fiber at each measurement. Figure 8(a) shows the transmission at selected frequencies in the first band gap as function of fiber length. The slopes of the linear fits to these loss data give the propagation loss, as shown in Fig. 8(b), and the interception with the ordinate axis at zero propagation distance of the fit curve gives the coupling loss, as shown in Fig. 8(c). The error bars indicate the standard deviation of the fit parameters.

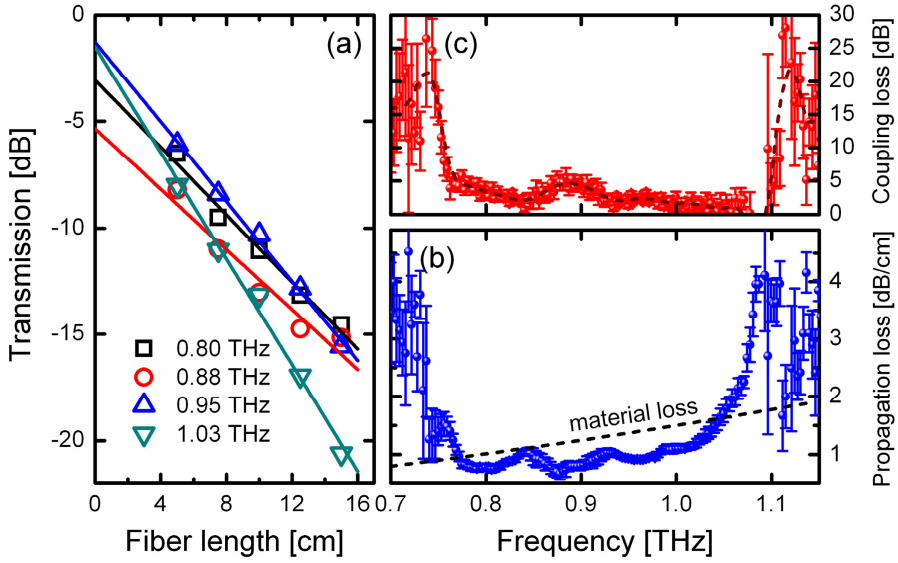

Fig. 8. (a) Relative transmission of the fiber with different lengths together with linear fits at four frequencies (0.8, 0.88, 0.95, 1.03 THz). (b) Frequency dependent propagation loss of the fiber (blue data markers) and material loss of TOPAS (quadratic fit - dashed line). (c) Coupling loss (red symbols) and solid line to guide the eye (running average of 5 data points).

We find a propagation loss, which is lower than the bulk material loss, as can be expected for the fundamental mode with a significant fraction of power residing within the air holes of the fiber. The modulation of the loss across the band gap is most probably caused by interference with cladding modes also observed in simulation (cf. Figure 4), as the cutback measurements were performed without attempting to attenuate the cladding modes. The frequency-dependent coupling loss shows a maximum of 5 dB at 0.88 THz, coinciding with the small dip in transmission seen in Fig. 6. Outside this region the coupling loss is 2-3 dB, consistent with the overlap integral between a free-space Gaussian beam profile and the fundamental mode of the first band gap (Fig. 3).

4. Conclusion

In conclusion, we have fabricated a low-loss porous-core honeycomb PBG THz fiber with a near perfect hole structure by drill-and-draw technology, and characterized the optical properties of the fiber with experimental THz-TDS techniques and numerical modelling. We

#177934 - $15.00 USD Received 11 Oct 2012; revised 30 Nov 2012; accepted 3 Dec 2012; published 19 Dec 2012

demonstrated that the fiber had a fundamental transmission band of 0.78-1.02 THz in which the loss is below 1.0 dB/cm, with the minimum loss of 0.7 dB/cm being at 0.88 THz. The manufactured fiber is not based on an optimized geometry, so we expect that the performance can be improved through optimizing fiber parameters, such as pitch and air-hole diameter.

Acknowledgments

We acknowledge technical assistance with simulations from Christian Agger and experiments from Krzysztof Iwaszczuk, both at DTU Fotonik.

#177934 - $15.00 USD Received 11 Oct 2012; revised 30 Nov 2012; accepted 3 Dec 2012; published 19 Dec 2012